Karla Knudson

USING AN UNCONVENTIONAL CLIMATE RECORD TO LINK GLACIMARINE SEDIMENTS TO TURBIDITE FREQUENCY IN THE NITINAT FAN, BRITISH COLUMBIA

Submitted for Publication in:

Marine Geology

in lieu of thesis in partial fulfillment
of the requirements for the degree of
Master of Science in Geology
Department of Geological Sciences
The University of Michigan

Accepted by:

Signature	Ingrid L. Hendy	8-8-08
Signature	Philip A. Meyers	8-7-08
Department Chair	Samuel B Mukasa	8-12-08

	Name	Date
	Name	Date
	Name	Date

Using an unconventional climate record to link glacimarine sediments to turbidite frequency in the Nitinat Fan, British Columbia

K.P. Knudson[1*] and I.L. Hendy[1]

---

[1] *University of Michigan*
Department of Geological Sciences
2534 C.C. Little Building
1100 N. University Avenue
Ann Arbor, MI 48109

[*]Corresponding author
E-mail: knudsonk@umich.edu
p: 734 615 2844 | f: 734 763 4690

Abstract

Continental margins in regions influenced by temperate ice sheets experience climate-dependent changes in sedimentary processes. A new stratigraphy is presented for Ocean Drilling Program Hole 888B, from the Nitinat Fan, on the Cascadia Margin, in which we examine the relationship between fluctuations in glacial-sourced sediment delivered to the continental shelf and turbidite frequency. Glacial/interglacial intervals were determined based on core lithology, $\delta^{18}O$ of planktonic foraminifera *Globigerina bulloides*, magnetic susceptibility, coiling ratios of foraminifera *Neogloboquadrina pachyderma,* and ^{14}C dates. We interpret the 240-meter-long core to represent Marine Isotope Stages (MIS) 2-4 (2-118 mbsf), MIS 5 (118-157 mbsf), and MIS 6 (213-240 mbsf). Using the MIS time constraints, we estimate sedimentation rates and turbidite frequencies, showing sedimentation rates for the Nitinat Fan were greatest during glacial intervals (MIS 2-4 and 6).

These results indicate that transport of glacimarine sediment to the continental slope promotes turbidity currents that are responsible for the most significant amount of offshore sedimentation. Thus, ODP Hole 888B, while strongly influenced by the local climatic conditions, cannot be interpreted in the same manner as a typical climate record, since deposition of this record was not continuous. Instead, this record is dominated by sediment deposited during glacial conditions and contains unconformities due to both non-deposition and turbidity current erosion.

Additionally, we find evidence for the influence of bacterial activity on post-depositional $\delta^{13}C$ precipitation within the sediments. The $\delta^{13}C$ values of *G. bulloides*

display negative spikes (up to -6.5‰) during MIS 2-4 and 6 that appear to be correlated with high methane concentrations, possibly indirectly related to glacial activity. Glaciers probably transported coarse-grained and organic material to the site, facilitating lateral methane flow and providing decomposable organic material to stimulate bacterial sulfate reduction to the point of methanogenesis.

Keywords: turbidite; turbidity current; glacimarine; Cordilleran; Cascadia Margin; Nitinat Fan

1. Introduction

This study investigates the climate-dependant changes in sedimentary processes at the Cascadia Margin by focusing on the turbidite record. At high latitudes during glacial intervals, sediment production and transport by ice sheets has the potential to deliver large sediment loads to the edge of the continental shelf. It is well known that phenomena such as earthquakes and storms may trigger turbidity currents; however, high continental shelf sedimentation rates may also promote slope instability leading to turbidity currents. Since proximate ice sheets increase continental slope sedimentation rates, it is possible that ice sheets also promote turbidity currents—which carry sediment from the shelf to sediment fans—indirectly affecting sedimentation further offshore. During non-glaciated intervals, the supply of sediment to the continental slope diminishes greatly such that turbidity currents become infrequent, even as the potential triggering mechanisms remain constant. Therefore, although a complex challenge, an improved understanding of the relationship between glacial activity on continental margins and turbidite sequence emplacement will improve our ability to employ turbidite records to interpret sediment depositional and tectonic settings in the past.

Previous studies of glacial-sourced turbidites, such as those deposited in the Cascadia Basin, are limited. To date, most turbidite studies have focused on temperate-latitude turbidite settings, which mainly receive a constant influx of sediments from rivers and greatly differ from high-latitude turbidite settings, which receive sporadic sedimentation. The limited work on high-latitude turbidites includes studies of the modern sedimentary setting of Antarctica (Wright and Anderson, 1982; Anderson et al., 1986; Escutia et al., 2000) and Alaska (Powell, 1983; Powell, 1990; Schwab and Lee, 1983; Domack, 1983). Of these locations, the regions of temperate glaciers in modern Alaska may be most similar to the Cascadia Margin during the last glacial (Powell, 1983). In Alaska, relationships between ice, ocean, and meltwater control sedimentary lithofacies, including gravity flow deposits characterized by interstratified sand and mud (Powell, 1983). Powell (1983) finds that modern turbidity currents are caused by subaqueous slumping that can be attributed to ice calving, cyclic wave loading, ice-push episodes, high sedimentation rates, glacier sliding, and/or earthquakes. Studies of Alaska have also found that sediment is mostly deposited during glacial stages (Carlson et al., 1990). During glacial maxima, glacial lobes reached the shelf edge, depositing sediment in the forms of moraines and ice rafted debris (Carlson et al., 1990). At the shelf edge, sediment would have been capable of slumping and sliding (Carlson et al., 1990), a prerequisite for turbidity currents.

Additionally, some turbidite studies have focused on Antarctica, although this depositional setting differs from that of Cascadia Margin during the last glacial, since Antarctica is presently covered by a permanent (not temperate) ice sheet. Anderson et al. (1986) found that the Weddell Fan, Antarctica, contains turbidite sands with

characteristics reflecting glaciofluvial and/or coastal processes, leading them to speculate that the sediment was mainly deposited during temperate glacial conditions—conditions perhaps like those experienced by the Cascadia Margin during the last glacial. Investigating the Antarctic Wilkes Land turbidites, Escutia et al. (2000) demonstrated important morphological differences in the character of glacial-sourced turbidite sediment fans compared with typical river-sourced fans, including a complex network of multiple tributary channels, greater channel relief, and pronounced fan gradients. Escutia et al. (2000) attributed the increased channel relief and fan gradients to the high volumes of sediment deposition on the continental shelf by "ice streams" during glacial maxima.

In this paper, we analyze a mid-latitude core record from Ocean Drilling Program (ODP) Site 888B, located offshore of the Cascadia Margin, within the Nitinat Fan (Fig. 1). The site's proximity to the Cordilleran Ice Sheet during the last glacial (Fig. 1) makes this location ideal for studying the effects of a glacial-sourced turbidite record. Previous studies have shown that these sediment fans receive most coarse-grained sediments via turbidity currents (Stokke et al., 1977 and references therein). Within the Cascadia Basin, Griggs and Kulm (1970) found that there were characteristic differences between Pleistocene (glacial) and Holocene (interglacial) turbidites. Additionally, some studies of the Nitinat Fan, such as Goldfinger et al. (2003), have focused on the role of cyclic earthquake-triggered turbidity currents during the Holocene. Yet, these studies do not demonstrate the connection between the sediment fluxes brought by glacier advance and increased turbidite frequency.

This study seeks to contribute to a better understanding of the processes affecting turbidite emplacement in the Nitinat Fan by identifying the source and timing of turbidite

sequences in the fan and relating this information to sediment characteristics within ODP Hole 888B. Specifically, the objectives of this study were: Firstly, to constrain the relative timing of turbidity current activity to specific Marine Isotope Stages (MIS) in order to determine if increased amounts of sediment were delivered to the site during glacial intervals. Secondly, to determine if relative turbidite frequency changed between intervals of glacial activity and ice free intervals. Finally, to resolve if this relationship between glacial-sourced sediments and turbidity current activity influenced the physical and chemical characteristics of sediments such that it affected microbe activity within the Nitinat Fan.

2. Geologic Setting

2.1 Tectonic influences

ODP Site 888B is located in the Cascadia Basin, which is greatly influenced by its unique tectonic setting. The Cascadia subduction zone, between the North American and Juan de Fuca plates, serves as the eastern border of the basin, and the Juan de Fuca and Gorda ridges form the western border (Fig. 1). Site 888B is situated 7 km seaward (west) of the accretionary wedge, which creates the continental slope; however the site is sufficiently distal from the wedge that deposited sediments are not deformed (Scientific Shipboard Party, 1994). Within the Cascadia Basin, there are two prominent sediment fans, which are the Nitinat Fan (Fig. 1) and the southerly adjoined Astoria Fan. The proximity of these fans to the Cascadia subduction zone causes local sedimentary depositional processes to be influenced by allocyclic forcing—such as earthquakes, tectonic uplift, variations in glacio-eustatic sea level, and volcanic activity (Underwood et al., 2005).

2.2 Sediment transportation via submarine channels

Sediment currently deposited in the Cascadia Basin is primarily composed of terrestrial material delivered by rivers draining onto the continental shelf (Griggs and Kulm, 1970; Crawford and Thompson, 1991). Upon deposition to the shelf, a network of submarine channels is responsible for much of the sediment delivery via turbidity currents across the continental margin to the Nitinat and Astoria Fans (Fig. 1; Griggs and Kulm, 1970; Underwood and Hoke, 2000; Underwood et al., 2005). The significant channels include the 2200-km-long Cascadia Channel, the Pacific Ocean's most major deep-sea channel (Griggs and Kulm, 1970). The Cascadia Channel is fed by several tributaries that begin on the continental slope by Washington state and flow through the Nitinat and Astoria fans (Fig. 1; Griggs and Kulm, 1970). The second major channel on the fan is the Vancouver Valley, which begins near the shelf of Vancouver Island and intersects the Juan de Fuca Channel in the northern part of the basin (Fig. 1). These channels have maximum depths of 70 km (Underwood and Hoke, 2000). Sediments carried in these submarine canyons are mainly deposited within the Nitinat Fan, particularly in the northern portion of the fan and in the Cascadia Channel (Stokke et al., 1977). Sedimentation rates at these focal locations are estimated to be 5-12 mg/cm^2 of sediment per year (Stokke et al., 1977).

3. Methods

3.1 Stable isotopes

From ODP Hole 888B, 301 sediment samples, each 2 cm thick, were taken at intervals of ~50 cm downcore from 2.125 to 232.3 mbsf, except where there was no core recovery (within 160 to 220 mbsf). Samples were washed with deionized water through a

63 μm mesh sieve, and the coarser faction was dried and weighed. From the >250 μm faction of each sample, five to twelve specimens of the planktonic foraminifera *Globigerina bulloides* were hand-picked and prepared following standard procedures. Stable oxygen and carbon isotopes were measured on a Finnigan MAT 251 Mass Spectrometer connected to a Kiel device. Analytical precision was better than 0.1‰. A best-fit regression line generated by the NBS-19 was used to correct ^{17}O data for acid fractionation and source mixing. All data are reported relative to the Vienna Pee Dee Belemnite (PDB) standard.

3.2 Radiocarbon dating

Radiocarbon dating was undertaken on mixed planktonic foraminifera (predominantly *G. bulloides* and *Neogloboquadrina pachyderma*) carbonate from two samples (ODP Hole 888 1H-03 45-47 cm and 5H-05 15-17 cm) at depths 3.4 and 40.15 mbsf, respectively. Samples were prepared using standard procedures (Guilderson et al., 2003) and were analyzed at the University of Arizona in the NSF Arizona Accelerator Mass Spectrometry Laboratory. Radiocarbon ages are reported as conventional ^{14}C kyr B.P. using the Libby half-life of 5,568 years following the conventions defined by (Stuiver and Polach, 1977) and include a background correction based on ^{14}C-free calcite and a standard $\delta^{13}C$ correction. The radiocarbon date for the upper-most sample at 3.4 mbsf yielded a radiocarbon age of 11,180 ± 210 ^{14}C yrs B.P. This date, in relation to the rest of the core, is illustrated in Fig. 2. The sample (5H-05 15-17 cm) from 40.15 mbsf did not produce a radiocarbon date, either because the sample size was too small or the sample age was beyond the radiocarbon scale. A regional reservoir correction, ΔR of 402 ± 50 years, has been assumed based on the closest ΔR measurement near the entrance of

the Strait of Juan de Fuca (Robinson and Thompson, 1981). Thus, incorporating the reservoir effect, the sediment at 3.4 mbsf is dated at 10,370 ^{14}C kyr B.P. or 12.28 ka. Reservoir-corrected ^{14}C dates younger than 22 ^{14}C kyr BP were calibrated using CALIB04 (Stuiver, et al., 2004) and the ^{14}C calibration dataset MARINE04 (Hughen, et al., 2004).

3.3 Magnetic susceptibility and lithology

Magnetic susceptibility and lithology were taken by ODP Leg 146 Shipboard Scientific Party (1994) following standard coring procedures. Grain size and color were determined for the entire core, except for the top 2 meters, which were removed for sampling prior to description (Scientific Shipboard Party, 1994). Grain size, defining each lithofacies, was determined using the Udden-Wentworth scale, and color—hue and chroma—was found using Munsell soil-color charts (Scientific Shipboard Party, 1994). Additionally, the Shipboard Scientific Party determined the coiling direction (sinistral versus dextral) of foraminifera *N. pachyderma* in 76 samples, at depths between 5.4-563.1 mbsf (Zellers, 1995). From henceforth dextral *N. pachyderma* will be referred to as *N. incompta* based on recent genetic analysis that has revealed these two morphotypes are actually different species (Darling et al., 2006). The ratio of sinistral *N. pachyderma* to dextral *N. incompta* at each depth is expressed as a percent.

4. Results

4.1 Lithology

Lithostratigraphic Unit I (0-148 mbsf) is composed of gray or dark greenish gray clayey silt interbedded with gray or dark gray fine to medium-grained sand. The upper sections (148-186 mbsf) of Unit II (148 to 440 mbsf) consist of fine-grained greenish

gray sand and greenish gray clayey silt. The mid sections of Unit II (downcore to 300 mbsf) are dark greenish gray fine to medium-grained sand and silty clay.

Overall, the lithology of the core is primarily silty clay/clayey silt with a relatively smaller proportion of sand (Fig. 2). Exceptions occur where there is a larger proportion of sand relative to silty clay/clayey silt (55-57, 65-68, 72-78, and 215-216 mbsf) , and where the sediments are entirely composed of sand (110-112, 115-119, 216-225, and 234-240 mbsf). Additionally, there is one isolated interval of silty sand/sandy silt at 212-216 mbsf. Gravel/dropstones are found at 19 mbsf, within a layer of predominately (two-thirds) silty clay/clayey silt and smaller amounts of sand. Gravel/dropstones reoccur at 57 mbsf, in a facies dominated by sand (~90%) with smaller proportions of silty clay/clayey silt. Core recovery was poor between 160-212 mbsf. Several meters of core were not recovered as shown in Fig. 2.

4.2 Stable Isotopes

Carbon isotopes ($\delta^{13}C$) in planktonic foraminifera such as *G. bulloides* are primarily a reflection of the organic carbon concentrations found in the foraminifera's environment and vital effects (Berger and Vincent, 1986a). Decreases in $\delta^{13}C$ in seawater (reflected by decreases in foraminiferal $\delta^{13}C$) indicate increased ^{12}C addition by organic carbon degradation associated with nutrient influx from upwelling events (Hemleben and Bijma, 1993). Additionally, very negative $\delta^{13}C$ can reflect secondary calcification from carbonate precipitated on foraminifera tests after deposition (Torres et al., 2003). The $\delta^{13}C$ isotope values primarily lie between -1.2‰ and -0.5, with some notable excursions (-6.5‰ and -3.0‰) at 110 and 115 mbsf, as well as one excursion (-3.5‰) at 225 mbsf (Fig. 2 and 3). Additionally, gradual changes occur in the top 25 m of the core, as $\delta^{13}C$

values become increasingly negative, fluctuating between -0.30 and 0.80‰ upcore of 8 mbsf and between -1.37 and -0.2‰ near 25 mbsf. Another gradual shift occurs between 87 and 105 mbsf, where $\delta^{13}C$ values become overall less negative. From 86.52-86.92 mbsf, $\delta^{13}C$ fluctuates from more negative values of -0.81‰ to less negative values of -0.61‰. $\delta^{13}C$ values from 104.77-105.56 mbsf increase from -0.15 to 0.20‰. Following this gradual shift, there is a marked shift towards more negative $\delta^{13}C$ values, beginning with the largest excursion (-6.5‰).

$\delta^{18}O$ in planktonic foraminifera is an indicator of ice volume, salinity, and temperature. Here we interpret decreases in $\delta^{18}O$ to indicate increases in temperature and decreases in ice volume. The oxygen ($\delta^{18}O$) isotope values range from 0 to 3.75‰ (Fig. 2). The top 20 m display a gradual increase in $\delta^{18}O$, as values at the top of the core range between 1.76‰ (3 mbsf) and 2.51‰ (4.5 mbsf) and deeper depths range between 2.90‰ (17.2) and 3.12‰ (18.1 mbsf). From 20 to 118 mbsf, $\delta^{18}O$ fluctuates around 3.0‰ and typically varies by no more than 1‰; however, an abrupt decrease in $\delta^{18}O$ from 2.85 to 1.13‰ occurs immediately after 118 mbsf. Additionally, after 118 mbsf, values show more variability (varying up to more than 1‰ within ~1 m between 127.17-128.45 mbsf) and fluctuate around 1.5‰. Poor core recovery and sandy sediments downcore from 155 mbsf have resulted in no *G. bulloides* data until 227 mbsf, at which point $\delta^{18}O$ increases again to ~2.5‰.

4.3 Magnetic Susceptibility

Magnetic susceptibility is a reflection of the concentration of magnetic minerals within the sediment and can be influenced by variations in lithogenic material—such as composition, relative abundance versus biogenic sediment, grain size, and grain shape.

ODP Hole 888B displays magnetic susceptibility values ranging from 17 S.I. (at 39.995 mbsf) to 1300 S.I. (at 8.997 mbsf), with the majority between 200 and 500 S.I. (Fig. 2). Many of the largest sustained peaks, at 55, 67, 103, and 150 mbsf, correlate with changes in lithology from a facies dominated by silty clay/clayey silt to sand. Between 2.145 and 97 mbsf, magnetic susceptibility values are almost never below ~150 S.I. and show great variability, regularly reaching values of 500 S.I. or greater several times within 10-m intervals. From 97.997-103.026 mbsf, the baseline for the lowest values is gradually raised from 312 to 960 S.I., although the high values (up to 960 S.I.) during this interval are comparable to the high values upcore of 97 mbsf. From 103.026-108.596, the baseline for the lowest values decreases to 698 S.I. After this point, there is a sharp decrease to 50 S.I. within less than 1 m (at 108.645 mbsf), which correlates with a change in facies from half sand and silty clay/clayey silt to an all-sand facies. Between 120 and 180 mbsf, variability is reduced. In this period, for the exception of a few punctuated peaks around 141, 142, 147, 165, and 171 mbsf, magnetic susceptibility values fluctuate by less than 200 S.I. within a 10-m interval, with most data ~300 S.I. At the bottom of the core, between 213 and 240 mbsf, variability increases, as values range from 87 to 876 S.I.

4.4 Planktonic Foraminiferal Faunal Response

In water temperatures below 8°C, the sinistral *N. pachyderma* predominates over the dextral *N. incompta*, which prefers water temperatures between 8° and 14°C (Reynolds and Thunell, 1986). The ratio of relative abundance of sinistral *N. pachyderma* to dextral *N. incompta* expressed as a percent, is plotted next to $\delta^{18}O$ in Fig. 4. The lowest value (69%) and most distinct peak occurs at 6.9 mbsf, when values deviate from the typical ratio values of ~93% at 5.4 mbsf. Additionally, a large shift (91-95%) occurs over

an interval from 130.6 mbsf to 167 mbsf, roughly in phase with a distinct decrease in $\delta^{18}O$ (0.6-2.2‰) that occurs between 128.45-141.37 mbsf.

5. Discussion

5.1 Glacial and Interglacial Core Characteristics

In order to reach our objective of identifying specific MIS within our core to determine relative interglacial and glacial sedimentation rates and turbidite frequency, it was necessary to use our proxies to determine the climatic conditions during each sediment facies. If sediments are coarse grained, reflect terrigenous input, contain high foraminiferal $\delta^{18}O$, and display high percentages of sinistral coiled *N. pachyderma* over dextral coiled *N. incompt*a, we assume sediments are indicative of glacial erosion and turbidity current deposition. In contrast, fine grained (silt and clay) sediments containing low foraminiferal $\delta^{18}O$ and increased abundance of *N. incompta* should correlate with other proxies characteristic of interglacial periods, when the shelf is sediment starved.

The sediment in the upper 250 mbsf of ODP Hole 888B appears to have been mostly deposited during glacial intervals. Specifically, sediment between 3.5 to 118 mbsf and between 213 to 240 mbsf contains physical and chemical characteristics of glacimarine sediment, while only the interval between 118-157 mbsf appears to have been deposited during an interglacial. (Insufficient core recovery between 157-213 mbsf prevents any interpretation). The evidence for the deposition of the upper 118 mbsf of sediment during the last glacial includes high (up to 1300 S.I. at 9.0 mbsf) magnetic susceptibility, indicative of significant input of lithogenic material relative to biogenic material (Fig. 2). High lithogenic input on what is presently a sediment starved continental margin (Macdonald and Pedersen, 1991) is strongly suggestive of a different

sediment production and transportation regime than at present. Glacial erosion and transportation would increase the sediment input to the continental slope. Additionally, the high abundance of sinistral *N. pachyderma*, between 98 and 100% (for the exception of one decline to 69% at 6.9 mbsf) relative to dextral *N. incompta* indicates the presence of cooler overlying surface water during sediment deposition (Fig. 4). Furthermore the high $\delta^{18}O$ of ~3.0‰ (Fig. 2 and 4), indicative of cooler temperatures and increased ice volumes, is similar to glacial $\delta^{18}O$ values found at nearby sites such as MD02-2496 (Hendy and Cosma, 2008). Throughout this interval, $\delta^{18}O$ varies by only ~1.1‰, indicating this sediment facies was deposited under similar (glacial) climate conditions. Finally, the date of 12.28 ka at 3.4 mbsf indicates that the sediment at that depth was deposited during MIS 1, yielding a sedimentation rate for the upper 3.4 mbsf of 28 cm/kyr.

The sediment between 3.5 and 118 mbsf was most likely deposited during MIS 4 to 2, (between 74 and 12 kyr B.P.; Martinson et al., 1987). If so, the sedimentation rate for this period is estimated to be 187 cm/kyr, which is similar to sedimentation rates for other locations on the Vancouver Island continental slope during the same time interval (Cosma et al., 2008). Radiocarbon dates show that sedimentation rates on the western Cascadia Abyssal Plain during the late Pleistocene were up to 170 cm/kyr, while sedimentation rates during the Holocene ranged from 2-3 and 8-10 cm/kyr on the western and eastern sides of the plain, respectively (Griggs et al., 1969).

Evidence for an unconformity appears ~118 mbsf, where an abrupt decrease in $\delta^{18}O$ from 2.85 to 1.13‰ coincides with a change in lithology from sand to silty clay (Fig. 2). This shift is interpreted as a break in sedimentation, which may be a result of

missing sediment due to erosion by turbidity current activity or non-deposition due to channel replumbing. Downcore of the unconformity, from 118 to 157 mbsf, the sediment displays non-glacial sediment characteristics (Fig. 2 and 4): relatively low magnetic susceptibility (no higher than 369 S.I., with only two exceptions of 547 S.I. at 142.3 mbsf and 1004 S.I. at 148.0 mbsf), relatively low ratios of sinistral *N. pachyderma* to dextral *N. incompta* (~90%), relatively low $\delta^{18}O$ (between 0.14 and 2.0‰), and finer grain size. This section of the core may represent MIS 5, which occurred between 130 and 74 kyr B.P. (Martinson et al., 1987).

From 213 to 240 mbsf (after ~50 m of discontinuous core recovery between 157-213 mbsf), the sediments again display characteristics of glacial conditions: high magnetic susceptibility values (as high as 876 S.I.; Fig. 2), high sinistral *N. pachyderma* percentages (98 to 100%), and low $\delta^{18}O$ values (between 2.2-2.75‰; Fig. 4). This section of the core likely represents another glacial period, possibly MIS 6, which occurred from 190 to 130 kyr B.P. (Martinson et al., 1987).

5.2 Turbidity currents as a source of sediment to the Cascadia Basin

In general, a turbidity current occurs when sediment accumulating on the continental slope is destabilized by over-steepening and/or an event such as an earthquake and is subsequently carried down slope by gravity. Clearly, the amount of sediment deposited on the continental slope plays a significant role in destabilizing slope sediments, although events—such as the more frequently examined earthquake events—may assist with destabilization. We argue that the frequency of turbidity currents depends on the amount of sediment available on the continental shelf, which, in regions of significant ice accumulation, are controlled by glacial erosion and transportation to the

shelf edge. Furthermore, in regions where ice accumulation occurs only during intervals of orbitally-driven global cooling, turbidite frequency is heavily influenced by sea level and whether an ice sheet existed in the region during cool intervals.

Our argument is supported by the following: (1) Continental slope sites demonstrate that sedimentation rates increased by an order of magnitude between the Holocene and the Last Glacial Maximum (Cosma et al., 2008; Kienast and McKay, 2001). (2) The change in sediment characteristics from hemipelagic to glacimarine indicates that the advance of the Cordilleran Ice Sheet was cause for the significant sedimentation rate increase. It stands to reason, therefore, that turbidite frequency would increase during glacial intervals in response to this increased sediment supply. Indeed, at ODP Hole 888B, sedimentation rates increased during the glacial MIS 2-4 and 6 (187 and 138 cm/kyr) compared with the interglacial MIS 5 (70 cm/kyr). Furthermore, the sediment deposited during the glacial intervals was generally coarse-grained (Fig. 2), requiring a high energy transportation process—deposition by turbidity currents. In contrast, the sediments in sections of the core associated with MIS 5 were dominantly silty clay/clayey silt (Fig. 2), suggesting a lower energy transportation process. In addition, turbidite frequency was determined by subjectively counting sand layers (Shipboard Scientific Party, 1994), and sand layers increased during glacial MIS 2-4 compared with interglacial MIS 5 suggesting increased turbidity current frequency.

5.3 Glacial delivery of sediments

The increase in turbidite frequency during glacial periods can be attributed to the considerable amounts of excess sediment that were brought to the continental shelf by the growing Cordilleran Ice Sheet. During the last glacial, the Cordilleran Ice Sheet grew

southward from southwestern British Columbia toward the Olympic Mountains, where it divided into two lobes—one moving toward the Strait of Juan de Fuca, and one moving into the area between the Olympic Mountains and the Cascade Range (Porter and Swanson, 1998). The ice sheet reached its maximum at ~14,000 ^{14}C yr B.P. (Porter and Swanson, 1998). At this time, ice 2 km thick and 900 m wide blanketed the southern region of British Columbia (Clague and James, 2002). Mapping and evidence of erosion and scouring have shown that ice covered much of the continental shelf of western British Columbia and southwest Vancouver Island, with lobes continuing to the shelf edge and calving into the ocean (Clague and James, 2002; Booth, 1987; Herzer and Bornhold, 1982).

This extensive ice sheet eroded and transported large amounts of sediment onto the shelf, where sediment was deposited, enabling gravity-driven turbidity currents on the continental slope to deliver coarse-grained material to Site 888B (Fig. 5). Therefore, we observe coarse-grained material at 2-118 mbsf and coarse and fine interbedded grains between 213-240 mbsf, which correlate with high δ^{18}O, high magnetic susceptibility, and high percentages of sinistral *N. pachyderm*a (Fig. 2 and 3). In addition, ice sheets that reach the shelf edge and generate icebergs are able to transport larger, gravel-sized sediments and deposit them as dropstones (Fig. 5c). Dropstones observed at 19 and 57 mbsf provide evidence of such ice rafting (Fig. 2) and offer support for iceberg calving during glacial periods.

In contrast, the environment during the warmer Holocene was not as conducive to high sedimentation rates on the continental slope, and the decrease in sediment deposition resulted in a drastic reduction of turbidity currents (Griggs and Kulm, 1970; Nelson,

1976). Currently, turbidity currents deliver less sediment to the Cascadia Basin than they did during the Pleistocene, because the British Columbia shelf is presently starved of terrigenous sediment (Macdonald and Pedersen, 1991). As eustatic sea level rise during the early Holocene enveloped the continental shelf and the river mouths, stream gradients decreased and less sediment was transported to the continental margin via these sources (Griggs and Kulm, 1970; Nelson, 1976). Instead, sediment is now trapped in fjords, inlets, and other scoured basins evacuated by the retreated ice sheet.

Additionally, sediment contribution is limited from the Fraser and Columbia rivers, which contain the two most abundant sediment sources near Vancouver Island (Crawford and Thomson, 1991). The Fraser River flows into the Strait of Georgia, where most of the sediments sink (Crawford and Thomson, 1991). The sparse sediments which pass through the Strait of Georgia without sinking must then also flow through the 130-km-long Juan de Fuca Strait before entering the ocean (Crawford and Thomson, 1991). The estuarine circulation within the Juan de Fuca Strait is a further impediment, as the net water flow is landward (Johannessen et al., 2006). The Columbia River, the other chief source of sediment to the Cascadia Basin, discharges 12.2 $\times 10^6$ m^3 of sediment per year (Griggs et al., 1969). It supplies sediment to several submarine channels, including the 2200-km-long Cascadia Channel, which carries sediment from the continental slope across the Cascadia Abyssal Plain (Griggs et al., 1969; Griggs and Kulm, 1970; Underwood et al., 2005). Overall, while the Columbia River contributes marginally to the sedimentation of the Nitinat Fan, the fan cannot receive significant sedimentation without the turbidity currents that are facilitated by glacial erosion and transportation.

During intervals of high eustatic sea level, when sediment is scarce, coarse-grained sedimentation has been observed to occur with ~600-year periodicity (Underwood et al., 2005), in association with earthquakes (Goldfinger et al., 2003). In contrast, during the last glacial interval (5 to 118 mbsf) we estimate turbidity currents occurred with a periodicity of ~75 years and ~200 years during the last interglacial (118 to 157 mbsf). Thus turbidity currents were most active during intervals of low sea level, such as during the Last Glacial Maximum. As earthquake frequency has not been linked to climate and is therefore unlikely to have increased during cool climatic intervals, we suggest an alternative mechanism for slope destabilization during cool intervals. We believe that during these periods—due to large sediment loads and low sea level—smaller events, such as large storm waves or storm surges were capable of destabilizing over-steepened continental slopes (Underwood et al., 2005).

5.4 $\delta^{13}C$ of G. bulloides and methane headspace

While the $\delta^{13}C$ of marine carbonate is usually used as an indication of nutrient utilization and/or upwelling, the negative *G. bulloides* $\delta^{13}C$ shifts (up to -6.5‰) found at 110, 115, and 225 mbsf are too extreme to be explained by such processes. Instead, we posit that these spikes are a post-depositional diagenetic product of high methane concentrations found at depths in the core. Methane headspace measurements (Fig 3.) taken by the Shipboard Scientific Party (Whiticar and Hovland, 1995) show two peaks of methane headspace, one between 78 and 113 mbsf (93 ppmv), and the second after 185 to 240 mbsf (6863 ppmv). As these high concentrations have not been attributed to methane hydrates, other possibilities must be considered (Cragg et al., 1996; Bottrell et al., 2000).

The intervals of all-sand facies appear to be correlated to the peaks in methane headspace. From 110-112 and 115-119 mbsf, there is a lithofacies change to sediments composed entirely of sand sized material (Fig. 2). This lithofacies shift corresponds to a negative peak of $\delta^{13}C$ (‰) of *G. bulloides* at 110 mbsf, a positive headspace methane peak, and a region of sulfate depletion between 87-113 mbsf (Fig. 3; Cragg et al., 1996). In this region, the increases in both sulfate reduction and methanogenesis are believed to be the result of methane-consuming bacterial activity (Cragg et al., 1996). Cragg et al. (1996) has described two hypotheses for the causes of this bacterial activity: first, higher rates of local methanogenesis, as a result of increased organic carbon concentrations, possibly terrigenous in origin, and second, a lateral inflow of methane (CH_4).

The first hypothesis, local methanogenesis, could explain the first peak in methane headspace. This first peak (78-113 mbsf) occurs at a depth containing wood fragments (Cragg et al., 1996), and high proportions of sand. Our stratigraphic evidence suggests that the sand facies may have been deposited during an early glacial period (MIS 4), in which the advancing ice sheet carried an influx of terrigenous organic matter to the shelf. High accumulation of terrigenous organic carbon has been recorded during intervals when the Cordilleran Ice Sheet was proximal to the continental slope. These high amounts of terrigenous organic matter have been attributed to the erosion of lowland forest during ice sheet advance (Cosma and Hendy, in press; Chang et al., in review). Unlike marine organic matter, wood fragments would be capable of sinking through the water column without degrading quickly, and would result in an aggregation of large amounts of organic matter in the sediment. Decay at depths significantly below the sediment-water interface could consume oxidants to the point allowing methanogenesis

to occur, subsequently generating a peak in the CH_4 (Cragg et al., 1996). However, the second methane peak (185-240 mbsf) occurs in a sandy layer (Fig. 3) for which there is no evidence of terrigenous material. With a lack of terrigenous organic material here, the lateral flow hypothesis is preferable. It is possible that this porous sand layer allowed gases produced elsewhere to pass more readily through pore spaces, producing a local pocket of CH_4 (Cragg et al., 1996).

We attribute the correlation between the peaks of headspace methane and $\delta^{13}C$ to the anaerobic oxidation of methane mediated by bacterial activity within the sediments. It has been shown that lipid biomarkers of archaebacteria are highly depleted in ^{13}C as a result of two processes (Hinrichs et al., 1999; Boetius et al., 2000): (1) These bacteria favor the ^{12}C isotope as they mediate the anaerobic oxidation of methane, and (2) bacteria consume methane with $\delta^{13}C$ of -62 to -72‰. Thus, there is a 70% depletion of ^{13}C relative to the primary product (Boetius et al., 2000) during anaerobic oxidation of methane, which occurs through sulfate reduction as follows:

$$CH_4 + SO_4^{2-} \longrightarrow HCO_3^- + HS^- + H_2O$$

As a result, HCO_3^- in sediment porewaters in methanogenic environments is often depleted in ^{13}C.

Another result of methane oxidation in an anaerobic environment is the increase in porewater alkalinity, which subsequently drives carbonate precipitation (Boetius et al., 2000). Therefore, at depths within ODP Hole 888B where methane headspace peaks, it can be expected that there is increased methane-consuming bacterial activity, producing porewater ^{13}C depletion and increased alkalinity in sediment porewaters (Luff et al., 2005). Post-depositional precipitation of carbonate with extremely negative $\delta^{13}C$ (-60‰;

Hinrichs et al., 1999; Boetius et al., 2000) can easily bias foraminiferal carbonate (Torres et al., 2003) such that the primary calcite isotopic composition is lost.

In contrast to the findings of Hill et al. (2004), and in agreement with the results of Torres et al. (2003), we posit that concentric layers of carbonate precipitation occurred as post-depositional diagenesis on the foraminiferal remains within the sediments of ODP Site 888. We believe that the extremely negative $\delta^{13}C$ values at 110 mbsf (-6.5‰), 115 mbsf (-3.0‰) and 225 mbsf (-3.5‰) are attributable to this secondary calcification process, because the $\delta^{13}C$ values are too extreme to be the result of primary calcification by vital effects (Berger and Vincent, 1986a). Furthermore, these extremely negative $\delta^{13}C$ values occur at depths within the core where both methane and porewater sulfate are relatively high (Fig. 3), providing the primary reactants for anaerobic oxidation of methane. We predict that at these depths, the consequential high alkalinity could drive the precipitation of ^{13}C-depleted calcite on the foraminiferal tests, resulting in post-depositional diagenesis of calcite with very negative $\delta^{13}C$.

6. Conclusions

The analysis of grain size, $\delta^{18}O$ (‰) of *G. bulloides,* magnetic susceptibility, and the relative abundance of sinistral *N. pachyderma* to dextral *N. incompta* suggests the following Marine Isotope Stages for ODP Core 888B: (1) Glacial MIS 2 through 4, at depth 3.5-118 mbsf. (2) Interglacial MIS 5, at depth 118-157 mbsf. (3) Glacial MIS 6, at depth 213-240 mbsf. Based on this chronology, very high sedimentation rates can be found for glacial intervals (~187 cm/kyr) that can be attributed to the large sediment load carried to the continental slope by the erosive, advancing Cordilleran Ice Sheet. Our results show that glacial sourcing of sediments from the Cordilleran Ice Sheet was a

major factor in the increase in frequency of turbidity currents, and thus for the increase in sedimentation of the Nitinat Fan. In contrast, the sedimentation rate (~70 cm/kyr) and turbidite frequency was lower for the interglacial interval. We attribute this result to sediment being trapped in the fjords and inlets vacated by the Cordilleran Ice Sheet, and influenced by marine processes at high eustatic sea levels.

The influence of turbidity currents on the sedimentation rate at ODP Hole 888B is significant in that it causes the sediment record to be predominantly glacial. That is, most of the record was deposited by turbidity currents under glacial conditions, and therefore mostly contains characteristic glacial period signals. Therefore, while directly influenced by climatic conditions, this core can not be used as a "traditional" climate record. Instead, this core records climate effects through lithology and sedimentation rate. Moreover, the discrepancy in sedimentation location between glacial and interglacial periods carries implications for strategically targeting sites for marine sediment climate records. In contrast to fjord, strait, and inlet sedimentary environments, which yield the most complete interglacial sediment records, marine sediment fans in regions of temperate glaciation yield mostly glacial sediments. Furthermore, due to geologically instantaneous turbidity current activity, deposition is not constant. Rather, the turbulent and sporadic nature of turbidity currents leads to unconformities due to both erosion and non-deposition.

Additionally, the new chronology of ODP Hole 888B allowed us to evaluate the relationship between microbial activity and the physical and chemical characteristics of the sediments within Nitinat Fan. Isotopic analysis of surface-dwelling planktonic foraminifera *G. bulloides* produced significant $\delta^{13}C$ excursions (up to -6.5‰) at 110, 115,

and 225 mbsf that cannot be attributed to nutrient utilization or vital effects occurring prior to foraminiferal test deposition. The coincidence of these $\delta^{13}C$ excursions with increases in methane headspace suggests methane-consuming bacterial activity resulted in ^{13}C depletion and increased alkalinity in the porewater. This alkalinity drove post-depositional carbonate precipitation of calcite with extremely depleted ^{13}C. Therefore, the very negative signatures are a secondary calcification process. Porewater ^{13}C depletion at these depths was facilitated by sand layers of glacial origin, allowing lateral methane flow and the occurrence of these $\delta^{13}C$ excursions. Additionally, large amounts of glacially-derived terrigenous organic carbon (wood fragments), found in association with the sand, may have provided the fuel for high concentrations of methane. The presence of wood fragments deposited during MIS 2-4 suggests that ice sheets eroded high amounts of organic material and coarse-grained sediment and deposited them on the shelf, where turbidity currents subsequently deposited them in Nitinat Fan. Therefore, by providing coarse-grained and organic material to the site, ice sheets present during deposition are, in part, now responsible for present microbial activity at depth in ODP Hole 888B.

Acknowledgements

I.L.H. thanks the National Science Foundation (NSF Grant Number OCE-0425382 (Marine Geology and Geophysics) for financial support. Samples were provided by T.F. Pedersen with the assistance of the Natural Sciences and Engineering Research Council of Canada. We thank the personnel of L. Wingate, K. Kimm and E. Pettygrew for technical and laboratory assistance. Finally we would like to thank the Shipboard Scientific Party of the MD126/IMAGES VIII (MONA) Cruise of the R/V Marion Dufresne operated by the French Polar Institute (IPEV).

References

Anderson, J.B., Wright, R., Andrews, B., 1986. Weddell Fan and associated abyssal-plain, Antarctica: Morphology, sediment processes, and factors influencing sediment supply. Geo-Mar. Lett. 6, 121-129.

Berger, W.H., Vincent, E., 1986a. Deep-sea carbonates-reading the carbon-isotope signal. Geol. Rundsch. 75, 249-269.

Boetius, A., Ravenschlag, K., Schubert, C.J., Rickert, D., Widdel, F., Gieseke, A., Amann, R., Jorgensen, B.B., Witte, U., Pfannkuche, O., 2000. A marine microbial consortium apparently mediating anaerobic oxidation of methane. Nature. 407, 623-626.

Booth, D.B., 1987. Timing and processes of deglaciation along the southern margin of the Cordilleran ice sheet. In: Ruddiman, W. F., Wright, H. E., Jr. (Eds.), Geology of North America. Geological Society of America, pp. 71-90.

Bottrell, S.H., Parkes, R.J., Cragg, B.A., Raiswell, R., 2000. Isotopic evidence for anoxic pyrite oxidation and stimulation of bacterial sulphate reduction in marine sediments. J. Geol. Soc. 157, 711-714.

Carlson, P.R., Bruns, T.R., Fisher, M.A., 1990. Development of slope valleys in the glacimarine environment of a complex subduction zone, northern Gulf of Alaska. In: Dowdeswell, J. A., Scourse, J. D. (Eds.), Glacimarine Environments: Processes and Sediments. Geological Society Special Publication, pp. 139-153.

Clague, J.J., James, T.S., 2002. History and isostatic effects of the last ice sheet in southern British Columbia. Quat. Sci. Rev. 21, 71-87.

Chang, A.S., Pedersen, T.F., Hendy, I.L., in review. Late Quaternary paleoproductivity history on the Vancouver Island Margin, western Canada: Evidence from a multiproxy geochemical approach. Can. J. Earth Sci.

Cosma, T., Hendy, I.L., Chang, A., 2008. Chronological constraints on Cordilleran Ice Sheet glaciomarine sedimentation from core MD02-2496 off Vancouver Island (western Canada). Quat. Sci. Rev. 27, 941-955.

Cosma, T., Hendy, I.L., in press. Pleistocene glacimarine sedimentation on the continental slope off Vancouver Island, British Columbia. Mar. Geol.

Cragg, B.A., Parkes, R.J., Fry, J.C., Weightman, A.J., Rochelle, P.A., Maxwell, J.R., 1996. Bacterial populations and processes in sediments containing gas hydrates (ODP Leg 146: Cascadia Margin). Earth. Planet. Sci. Lett. 139, 497-507.

Crawford, W.R., Thomson, R.E., 1991. Physical Oceanography of the western Canadian continental-shelf. Cont. Shelf Res. 11, 669-683.

Darling, K., 2006. A resolution for the coiling direction paradox in Neogloboquadrina pachyderma. Paleoceanography. 21, PA2011.

Domack, E.W., 1983. Facies of Late Pleistocene Glacial-Marine Sediments on Whidbe Island, Washington: An Isostatic Glacial-Marine Sequence. In: Molnia, B. (Eds.), Glacial-Marine Sedimentation. Plenum Press, pp. 535-570.

Escutia, C., Eittreim, S.L., Cooper, A.K., Nelson, C.H., 2000. Morphology and acoustic character of the Antarctic Wilkes land turbidite systems: Ice-sheet-sourced versus river-sourced fans. J. Sediment. Res. 70, 84-93.

Goldfinger, C., Nelson, C.H., Johnson, J.E., 2003. Deep-water turbidites as Holocene earthquake proxies: the Cascadia subduction zone and Northern San Andreas Fault systems. Ann. of Geophys. 46, 1169-1194.

Griggs, G.B., Carey, A.G., Jr., Kulm, L.D., 1969. Deep-sea sedimentation and sediment-fauna interaction in Cascadia channel and on Cascadia abyssal plain. Deep-Sea Res. Oceaongr. Abstr. 16, 157-170.

Griggs, G.B., Kulm, L.D., 1970. Sedimentation in Cascadia deep-sea channel. Geol. Soc. Am. Bull. 81, 1361-1384.

Guilderson, T.P., Southon, J.R., Brown, T.A., 2003. High-precision AMS C-14 results on TIRI/FIRI turbidite. Radiocarbon. 45, 75-80.

Hendy, I.L., Cosma, T., 2008. Vulnerability of the Cordilleran Ice Sheet to iceberg calving during late quaternary rapid climate change events - art. no. PA2101. Paleoceanography. 23, A2101-A2101.

Hemleben, C., Bijma, J., 1993. Foraminiferal population dynamics and stable carbon isotopes. NATO ASI Series. Series I: Global Environmental Change. 17. 145-166.

Herzer, R.H., Bornhold, B.D., 1982. Glaciation and post-glacial history of the continental-shelf off southwestern Vancouver Island, British-Columbia. Mar. Geol. 48, 285-319.

Hill, T.M., Kennett, J.P., Valentine, D.L., 2004. Isotopic evidence for the incorporation of methane-derived carbon into Foraminifera from modern methane seeps, Hydrate Ridge, Northeast Pacific. Geochim. Cosmochim. Acta. 68, 4619-4627.

Hinrichs, K.U., Hayes, J.M., Sylva, S.P., Brewer, P.G., DeLong, E.F., 1999. Methane-consuming archaebacteria in marine sediments. Nature. 398, 802-805.

Hughen, K.A., Baillie, M.G.L., Bard, E., Beck, J.W., Bertrand, C.J.H., Blackwell, P.G., Buck, C.E., Burr, G.S., Cutler, K.B., Damon, P.E., Edwards, R.L., Fairbanks, R.G., Friedrich, M., Guilderson, T.P., Kromer, B., McCormac, G., Manning, S., Ramsey, C.B., Reimer, P.J., Reimer, R.W., Remmele, S., Southon, J.R., Stuiver, M., Talamo, S., Taylor, F.W., van der Plicht, J., Weyhenmeyer, C.E., 2004. Marine04 marine radiocarbon age calibration, 0-26 cal kyr BP. Radiocarbon. 46, 1059-1086.

Johannessen, S.C., Masson, D., Macdonald, R.W., 2006. Distribution and cycling of suspended particles inferred from transmissivity in the Strait of Georgia, Haro Strait and Juan de Fuca Strait. Atmos.-Ocean. 44, 17-27.

Kienast, S. S., McKay, J. L. 2001. Sea surface temperatures in the subarctic Northeast Pacific reflect millennial-scale climate oscillations during the last 16 kyrs. Geophys. Res. Lett. 28, 1563-1566.

Luff, R., Greinert, J., Wallmann, K., Klaucke, I., Suess, E., 2005. Simulation of long-term feedbacks from authigenic carbonate crust formation at cold vent sites. Chem. Geol. 216, 157–174.

Macdonald, R.W., Pedersen, T.F., 1991. Geochemistry of sediments of the western Canadian continental shelf. Cont. Shelf Res. 11, 717-735.

Martinson, D.G., Pisias, N.G., Hays, J.D., Imbrie, J., Moore, T.C., Shackleton, N.J., 1987. Age dating and the orbital theory of the ice ages-Development of a high-resolution-0 to 300,000-year chronostratigraphy. Quat. Res. 27, 1-29.

Nelson, H., 1976. Late Pleistocene and Holocene depositional trends, processes, and history of Astoria deep-sea fan, northeast Pacific. Mar. Geol. 20, 129-173.

Porter, S.C., Swanson, T.W., 1998. Radiocarbon age constraints on rates of advance and retreat of the Puget lobe of the Cordilleran ice sheet during the last glaciation. Quat. Res. 50, 205-213.

Powell, R.D., 1983. Glacial-Marine Sedimentation Processes and Lithofacies of Temperate Tidewater Glaciers, Glacier Bay, Alaska. In: Molnia, B. (Eds.), Glacial Marine Sedimentation. Plenum Press, pp. 185-232.

Powell, R.D., 1990. Glacimarine processes at grounding-line fans and their growth to ice-contact deltas. In: Dowdeswell, J. A., Scourse, J. D. (Eds.), Glacimarine Environments: Processes and Sediments. Geological Society Special Publication, pp. 53-74.

Reynolds, L.A., Thunell, R.C., 1986. Seasonal production and morphological variation of neogloboquadrina-pachyderma (Ehrenberg) in the northeast Pacific. Micropalenotology. 32, 1-18.

Robinson, S. W., Thompson, G. 1981. Radiocarbon corrections for marine shell dates with application to southern Pacific Northwest coast prehistory. Syesis. 14, 45-57.

Schwab, W.C., Lee, H.M., 1983. Geotechnical Analyses of Submarine Landslides in Glacial Marine Sediment, Northeast Gulf of Alaska. In: Molnia, B. (Eds.), Glacial Marine Sedimentation. Plenum Press, pp. 145-184.

Shipboard Scientific Party, 1994. Site 888. In: Westbrook, G. K., Carson, B., Musgrave, R. J. (Eds.), Proceedings of the Ocean Drilling Program, Initial Reports, 146 (Pt. 1). Ocean Drilling Program, College Station, TX, pp. 55-125.

Stokke, P.R., Carson, B., Baker, E.T., 1977. Comparison of bottom nepheloid layer and late Holocene deposition on Nitinat Fan-Implications for lutite dispersal and deposition. Geol. Soc. of Am. Bull. 88, 1586-1592.

Stuiver, M., Polach, H. A. ,1977. Discussion and reporting of ^{14}C data, Radiocarbon. 19, 355-363.

Stuiver, M., Polach, H.A., 1977. Discussion and reporting of 14C data. Radiocarbon. 19, 355-363.

Stuiver, M., Reimer, P.J., Reimer, R.W., 2004. CALIB 4.0 <www.calib.org>.

Torres, M.E., Mix, A.C., Kinports, K., Haley, B., Klinkhammer, G.P., McManus, J., de Angelis, M.A., 2003. Is methane venting at the seafloor recorded by delta C-13 of benthic foraminifera shells? Paleoceanography. 18, 1-12.

Underwood, M.B., Hoke, K.D., 2000. Composition and provenance of turbidite sand and hemipelagic mud in northwestern Cascadia Basin. In: Fisher, A. D., Davis, E.E., Escutia, C. (Eds.), Proceedings of the Ocean Drilling Program, Scientific Results. Ocean Drilling Program, 168, pp. 51-65.

Underwood, M.B., Hoke, K.D., Fisher, A.T., Davis, E.E., Giambalvo, E., Zuhlsdorff, L., Spinelli, G.A., 2005. Provenance, stratigraphic architecture, and hydrogeologic influence of turbidites on the mid-ocean ridge flank of northwestern Cascadia Basin, Pacific Ocean. J. Sediment. Res. 75, 149-164.

Whiticar, M.J., Hovland, M., 1995. Data Report: Molecular and stable isotope analysis of sorbed and free hydrocarbon gases of Leg 146, Cascadia and Oregon Margins. In: Carson, B., Westbrook, G. K., Musgrave, R. J., Suess, E. (Eds.), Proceedings of

the Ocean Drilling Program, Scientific Results, 146 (Pt. 1). Ocean Drilling Program, College Station, TX, pp. 439-449.

Wright, R., Anderson, J.B., 1982. The importance of sediment gravity flow to sediment transport and sorting in a glacial marine environment: Eastern Weddell Sea, Antarctica. Geol. Soc. of Am. Bull. 93, 951-963.

Zellers, S.D., 1995. Foraminiferal biofacies, paleoenvironments, and biostratigraphy of Neogene-Quaternary sediments, Cascadia Margin. In: Carson, B., Westbrook, G. K., R.J., M., Suess, E. (Eds.), Proceedings of the Ocean Drilling Program, Scientific Results, 146 (Pt. 1). Ocean Drilling Program, College Station, TX, pp. 79-113.

Figure Captions

Figure 1. Map showing the location of Ocean Drilling Program (ODP) Hole 888B, the straits and channels that carry sediments to the Nitinat Fan (after Underwood et al., 2005), and the Cordilleran Ice Sheet position during glacial retreat (Clague and James, 2004).

Figure 2. Comparison of ODP Core 888B records of (a) core section numbers, (b) stratigraphic column showing lithology of the sediments, (c) $\delta^{13}C$ (‰) of *G. bulloides,* (d) $\delta^{18}O$ (‰) of *G. bulloides,* (e) magnetic susceptibility, and (f) ^{14}C dates and interpreted Marine Isotope Stages (white indicates glacial and gray indicates interglacial). A possible unconformity marked by a notable shift in the $\delta^{13}C$, $\delta^{18}O$, and magnetic susceptibility data, as well as an abrupt transition to an all-sand facies, is indicated by the dotted line.

Figure 3. Comparison of (a) $\delta^{13}C$ (‰) of *G. bulloides* with (b) headspace methane (ppmv) and sulfate (mM; Shipboard Scientific Party, 1994), as well as (c) lithology (Shipboard Scientific Party, 1994). Gray and white bands indicate interglacial and glacial intervals, respectively.

Figure 4. Comparison of (a) $\delta^{18}O$ (‰) of *G. bulloides* and (b) ratio (%) of sinistral (left-coiling) *N. pachyderma* to dextral (right-coiling) *N. incompta* (Shipboard Scientific Party, 1994), as well as (c) lithology (Shipboard Scientific Party, 1994). Gray and white bands indicate interglacial and glacial intervals, respectively.

Figure 5. Sediment deposition from the edge of the continent to the ocean during (a) interglacial intervals occurs at a relatively slow rate, since many sediments are accumulated in fjords, straits, and sounds inland of the continental shelf. Sediments further seaward, on the continental slope, are slowly deposited by gravity. During (b) early glacial intervals, sedimentation is increased as ice sheets erode sediment beneath them and push sediment stored above the continental shelf towards the ocean. Turbidites are deposited on the continental rise when unsorted sediments reach the shelf break and flow down slope in turbidity currents. During (c) glacial maximum, the advanced ice sheets calve near the shore and carry unsorted sediments into the ocean as ice rafted debris (IRD) and deposit them as dropstones.

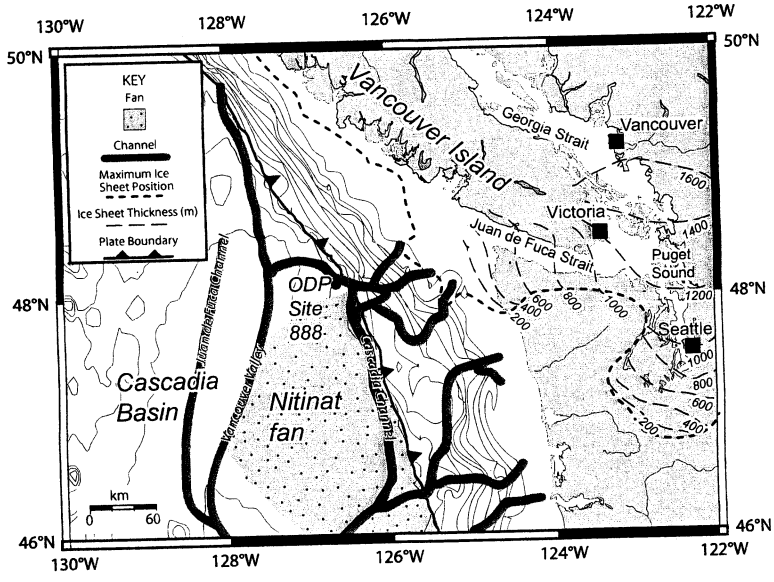
130°W
128°W
126°W
124°W
122°W
50°N
48°N
46°N
KEY
Fan
Channel
Maximum Ice Sheet Position
Ice Sheet Thickness (m)
Plate Boundary
Vancouver Island
Georgia Strait
Vancouver
Victoria
Juan de Fuca Strait
Puget Sound
Seattle
ODP Site 888
Cascadia Basin
Nitinat fan
Juan de Fuca Canyon
Vancouver Knoll
Cascadia Channel
1600
1400
1200
1000
800
600
400
200
km
0
60

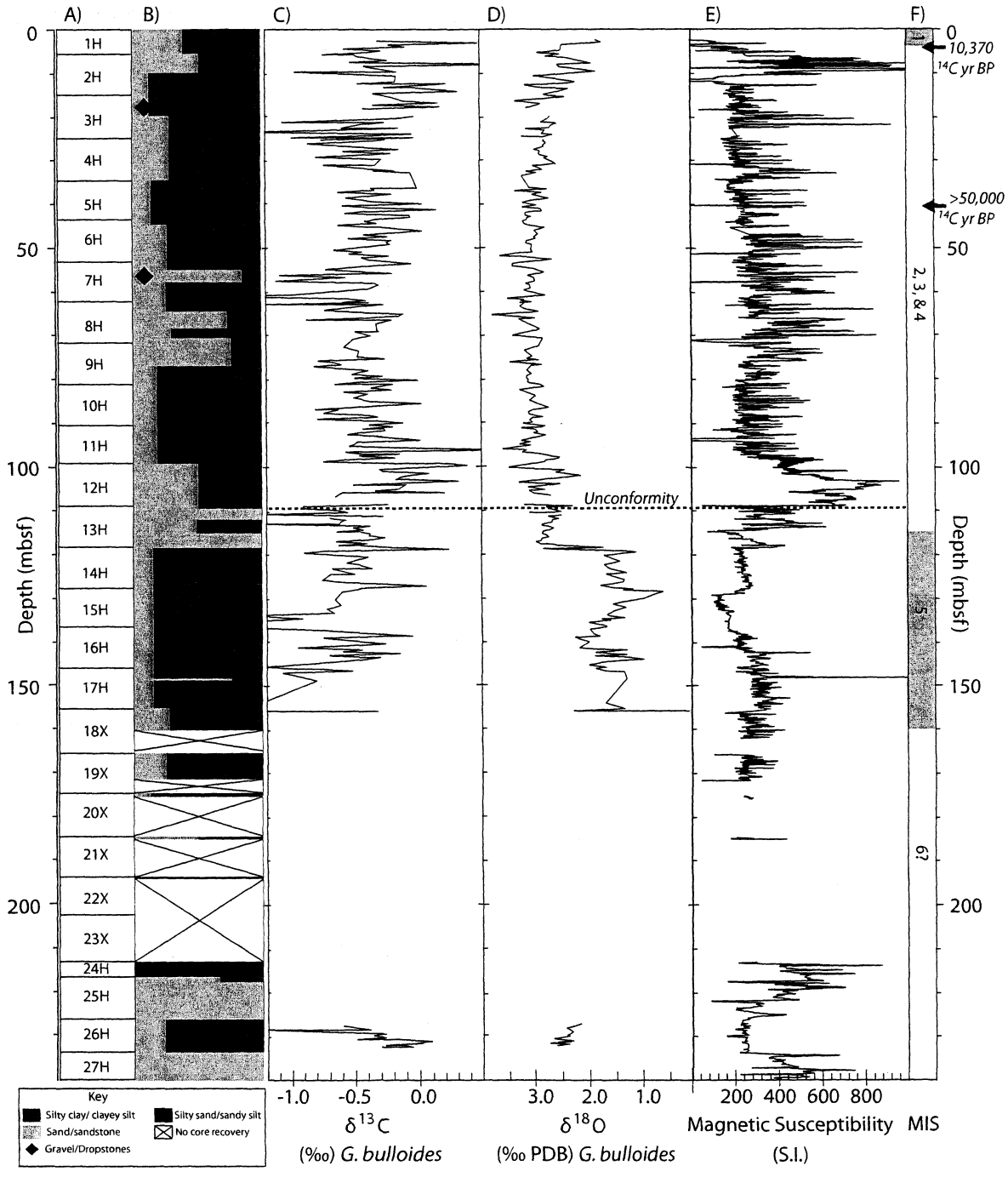
A)
B)
C)
D)
E)
F)
0
50
100
150
200
Depth (mbsf)
1H
2H
3H
4H
5H
6H
7H
8H
9H
10H
11H
12H
13H
14H
15H
16H
17H
18X
19X
20X
21X
22X
23X
24H
25H
26H
27H
Unconformity
10,370
14C yr BP
>50,000
14C yr BP
2, 3, & 4
5
6?
Key
Silty clay/ clayey silt
Silty sand/sandy silt
Sand/sandstone
No core recovery
Gravel/Dropstones
-1.0
-0.5
0.0
δ13C
(‰) G. bulloides
3.0
2.0
1.0
δ18O
(‰ PDB) G. bulloides
200
400
600
800
Magnetic Susceptibility
(S.I.)
MIS

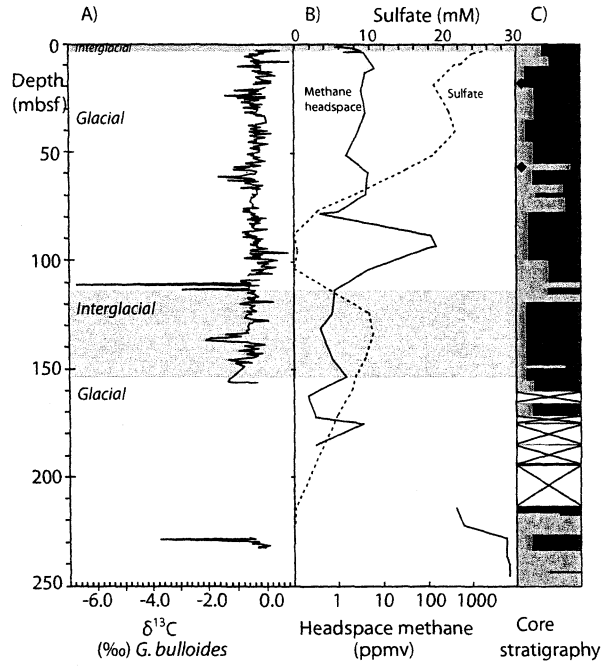
A)
B)
Sulfate (mM)
C)
0
10
20
30
Depth (mbsf)
Interglacial
Glacial
Methane headspace
Sulfate
50
100
Interglacial
150
Glacial
200
250
-6.0
-4.0
-2.0
0.0
1
10
100
1000
δ13C (‰) G. bulloides
Headspace methane (ppmv)
Core stratigraphy

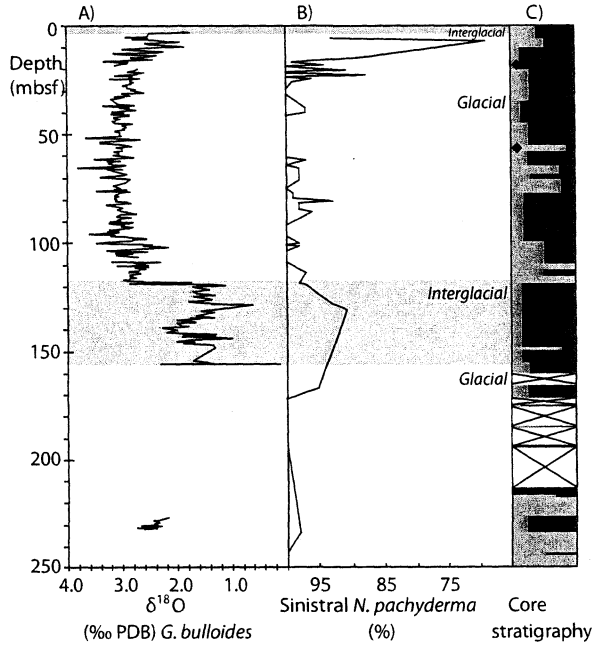
A)
B)
C)
0
50
100
150
200
250
Depth
(mbsf)
Interglacial
Glacial
Interglacial
Glacial
4.0
3.0
2.0
1.0
δ18O
(‰ PDB) G. bulloides
95
85
75
Sinistral N. pachyderma
(%)
Core
stratigraphy

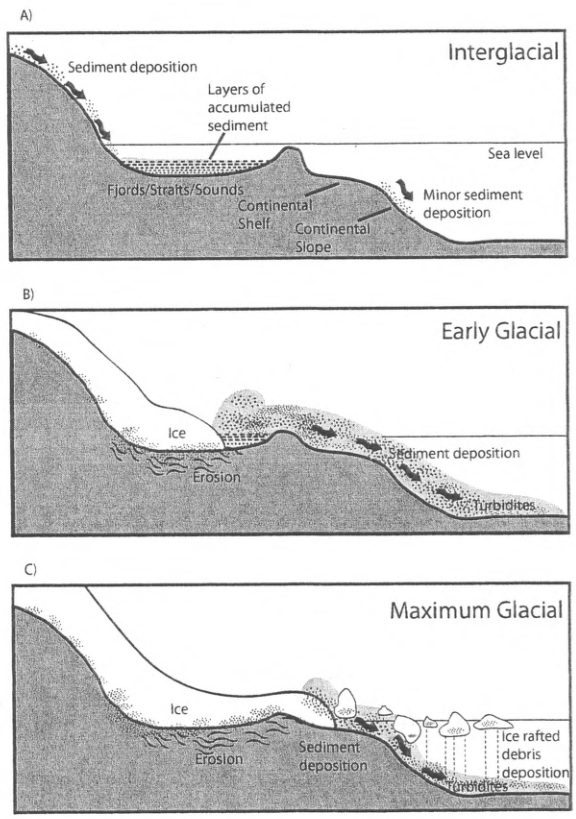
A)
Interglacial
Sediment deposition
Layers of accumulated sediment
Sea level
Fjords/Straits/Sounds
Continental Shelf
Continental Slope
Minor sediment deposition
B)
Early Glacial
Ice
Erosion
Sediment deposition
Turbidites
C)
Maximum Glacial
Ice
Erosion
Sediment deposition
Ice rafted debris deposition
Turbidites